Multiple ionization of noble gases by swift H_2^+ ions in breakup and nonbreakup collisions

G. M. Sigaud,[1,*] M. M. Sant'Anna,[2] H. Luna,[1] A. C. F. Santos,[2] C. McGrath,[3] M. B. Shah,[3]
E. G. Cavalcanti,[4] and E. C. Montenegro[1]

[1]*Departamento de Física, Pontifícia Universidade Católica do Rio de Janeiro, Caixa Postal 38071, Rio de Janeiro, RJ 22452-970, Brazil*
[2]*Instituto de Física, Universidade Federal do Rio de Janeiro, Caixa Postal 68528, Rio de Janeiro, RJ 21941-972, Brazil*
[3]*Department of Pure and Applied Physics, The Queen's University of Belfast, Belfast BT7 1NN, Northern Ireland, United Kingdom*
[4]*Instituto de Radioproteção e Dosimetria, Comissão Nacional de Energia Nuclear, Rio de Janeiro, RJ 22780-160, Brazil*

(Received 16 February 2004; published 28 June 2004)

We have measured multiple-ionization yields of He, Ne, Ar, Kr, and Xe targets by 1.0 MeV/amu H_2^+ molecular ions for both the dissociative and nondissociative channels. Except for the case of the breakup of the H_2^+ into two protons, we have also determined the absolute cross sections for the multiple ionization of the targets. The ratios of multiple to single ionization for the nondissociative channel are similar to those for equivelocity protons, which, however, are consistently smaller than those for the breakup channels, for all charge states and targets. A simple analysis, based on the independent particle model, considering postcollisional time-delayed ionization for the Ne and Ar targets, evinces the importance of these mechanisms in the target multiple ionization and of the antiscreening in collisions where the projectile electron undergoes a transition.

DOI: 10.1103/PhysRevA.69.062718 PACS number(s): 34.50.Fa, 52.20.Hv

I. INTRODUCTION

Since the pioneering theoretical work of Tuan and Gerjuoy in 1960 [1], there has been an appreciable amount of experiments involving collisions between ions as projectiles and neutral molecules as targets, in which the influence of the alignment of the molecular axis with respect to the projectile direction on processes such as target excitation, ionization, and fragmentation are studied [2–6]. More recently, measurements of alignment effects on electron capture from D_2^+ molecular ions by doubly charged atomic ions have been reported [7,8]. These alignment effects are closely related to the two-center nature of the molecular target and are usually measured by an appropriate angular selection of the dissociation fragments of the molecular target after the collision.

For dressed projectiles, an important process is the projectile ionization, usually called electron loss. The effects of the two-center nature of a molecular target on the projectile electron loss have also been shown, both theoretically [9] and experimentally [10]. In the projectile frame, the electron loss is due to the action of the incoming target. Thus, an equivalent way of studying experimentally the influence of both the alignment of the molecular axis and the two-center nature of the molecule on electron excitation and ionization is to use molecular ions as projectiles impinging upon neutral atomic targets.

In collisions where the projectiles are one-electron molecular ions and the targets are neutral atoms, the breakup and nonbreakup exit channels for the projectile are signatures, respectively, of the occurrence or not of the excitation or loss of the projectile electron. For the nondissociative channel, it should be expected that target multiple ionizations, were dominated by contributions from large impact parameters. In close collisions, the molecular ion is less likely to survive as such, since, as the projectile penetrates the atomic electron cloud, it is subject to higher fields, thus increasing the molecular ionization or dissociation. Besides this, since a molecular ion is a dressed projectile, there is an additional source for dissociation due to the greater overlap of the projectile and target electron clouds: the two-center electron-electron dynamical correlation, called antiscreening, which can play a very important role—at intermediate and high velocities—because it gives rise to the simultaneous excitation and/or ionization of both collision partners [11].

From the target point of view, its multiple ionization is due to the contributions of different mechanisms, including (i) the direct ionization of outer-shell electrons, (ii) multiple charge transfer, and (iii) inner-shell ionization followed by time-delayed postcollisional electron emission [12,13]. Thus, it is clear that the number of electrons—and which ones—which are most likely to participate in the process is an important question to be answered.

In this paper, we report on coincidence measurements of the multiple ionization of noble gases in collisions with 1 MeV/amu H_2^+ molecular ions, for both the dissociative and nondissociative channels. In two cases we present absolute multiple-ionization cross sections for the targets: the nonbreakup channel and the breakup channel which gives $H+H^+$ as reaction products. For the dissociative channel with Coulomb explosion, giving H^++H^+ as final products, we had to restrict ourselves to projectiles whose spatial orientation was parallel to the beam axis. Thus, for this exit channel, only relative results are presented. The measurement of both dissociation channels can, then, provide information about the influence of the molecular alignment on the target multiple ionization.

In a previous paper [14], we discussed some aspects concerning the differences between the breakup and nonbreakup channels in collisions of H_2^+ with Ne targets. Analysis of the relative multiple-ionization yields showed that the non-

*Electronic address: gms@vdg.fis.puc-rio.br

 ©2004 The American Physical Society

breakup channel produces similar results than equivelocity protons, while the breakup channels lead to charge-state distributions close to the measured Ne $2s^{-1}$ postcollisional decay distribution from photoionization. Here, for the nondissociative channel we observe that the absolute single-ionization cross sections saturate as the target atomic number increases, as has been reported before for projectile electron loss [15–17] and target multiple ionization by other projectiles [18]. We also perform a more detailed analysis of Ne and the more complicated Ar targets, including shake-off transitions, in a similar way as in [12], but using more accurate single-electron probabilities for both the nondissociative and dissociative channels. In the latter, we included the antiscreening contribution, in a way similar to that suggested by Sant'Anna *et al.* [19]. Our analyses point towards the conclusion that the interaction between the H_2^+ electron and the target electrons plays a major role in the dissociation channels, thus supporting the idea, discussed in [14], that sequential ionization of the target by the projectile fragments plays a minor role.

The paper is organized as follows. In Sec. II, the experimental setup is briefly described. In Sec. III, we present absolute and relative multiple-ionization cross sections for all possible final states of the projectile and compare them with data from proton and electron projectiles. In this section, we also present calculations based on the independent particle model (IPM), including time-delayed postcollisional transitions, for the Ne and Ar targets, and compare them with the experimental data. Finally, some conclusions are drawn in Sec. IV.

II. EXPERIMENT

The experiment was carried out at the 4.0-MV Van de Graaff accelerator of the Catholic University of Rio de Janeiro. The experimental setup has been already described in Refs. [14,19], and only its main features will be presented here. A beam of 1 MeV/amu H_2^+ is momentum analyzed by two magnets and passes through a gas chamber, whose pressure is absolutely measured by a capacitive manometer. The emergent charged beams—namely, H_2^+ and H^+—are separated by a second magnet and detected 4 m downstream. The geometrical distribution of the projectiles reaching the detection chamber was analyzed by an *x*-*y* position-sensitive microchannel plate (MCP) detector, with a sensitive area of 40 mm. The protons produced in the breakup collisions have two different ranges of angular spread [20]. For the $H_2^+ + A \rightarrow H^+ + H^0 + A^{q+}$ channel there is no significant molecular explosion, the effective scattering angle is small, and only a negligible number of H^+ ions falls outside a 4-mm-diam circle regardless of the original spatial orientation of the molecular ion projectile. On the other hand, for the $H_2^+ + A \rightarrow H^+ + H^+ + A^{q+}$ channel, there is a Coulomb explosion between the molecular fragments, so that the same detection area defines a cone with an acceptance angle of 10° around the beam axis, in the projectile center-of-mass frame [21]. Thus, only fragments corresponding to the molecular projectiles originally aligned with the beam axis were detected for the $H^+ + A^{q+}$ exit channel. As a consequence, this was the only exit channel for which we could not measure absolute-cross sections.

TABLE I. Absolute multiple-ionization cross sections of noble gases by H_2^+ ions: nondissociative channel (Mb).

q	He	Ne[a]	Ar	Kr	Xe
1	20.9±2.14	62.6±6.42	107±11	81.2±8.38	96.5±10.0
2	0.10±0.029	2.79±0.32	6.50±0.82	7.67±0.87	19.1±2.15
3		0.12±0.06	1.09±0.27	4.40±0.54	5.30±0.70
4			0.45±0.18	0.65±0.21	3.63±0.52
5				0.22±0.20	0.48±0.32

[a]Reference [14].

These exit channels were detected by two 4-mm-diam surface-barrier detectors, one for the emergent H_2^+ and the other for the emergent H^+ ions. The breakup channels were separated in the following way. In the case of the $H_2^+ + A \rightarrow H^+ + H^0 + A^{q+}$ channel, only one proton is detected for each H_2^+ projectile, while in the $H_2^+ + A \rightarrow H^+ + H^+ + A^{q+}$ channel, the two emergent protons are detected together, resulting in a pulse 2 times higher than the former. Careful centralization of the H^+ beam on the surface barrier detector was important to avoid contamination between the breakup channels. The target recoil ions produced in the collision were analyzed by a time-of-flight (TOF) spectrometer in coincidence with the final state of the projectile. Details about the TOF apparatus are given elsewhere [18,22].

III. RESULTS AND DISCUSSION

Absolute cross sections for the multiple ionization of the noble gases from He to Xe by 1.0-MeV/amu H_2^+ ions are presented in Tables I and II for the exit channels of nondissociation of the molecular ion and of its dissociation into a proton and a neutral hydrogen atom, respectively. As mentioned above, due to the experimental detection conditions, we could not obtain absolute cross sections for the dissociative channel producing two protons. For this process, the yields for target multiple ionization relative to single ionization are presented in Table III.

In Fig. 1 our absolute single-ionization cross sections for the nondissociative channel (solid circles) as a function of the target atomic number are compared with the equivelocity proton data of Cavalcanti *et al.* [13] (open squares). One can see that, in both cases, there is a saturation of the cross sections as the target atomic number increases, more pronounced for the H_2^+ projectile than for protons. For protons, single ionization is suppressed due to the relative increase of the target multiple ionization, either directly or by means of time-delayed postcollisional ionization, as the number of target electrons increase [12]. In the present case, for the nonbreakup channel the only mechanism that can occur is direct ionization of the target electron by the screened nuclear field of the projectile molecular ion. Voitkiv *et al.* [16], analyzing the projectile electron loss of He^+ projectiles using a nonperturbative unitarized theory based on the sudden approximation, observed that, for close collisions, the probability of

TABLE II. Absolute multiple-ionization cross sections of noble gases by H_2^+ ions: dissociative H^0+H^+ channel (Mb).

q	He	Ne[a]	Ar	Kr	Xe
1	7.07±0.73	28.1±2.9	29.6±2.97	23.6±2.44	23.2±2.42
2	0.15±0.023	4.13±0.46	5.88±0.64	7.10±0.76	13.6±1.47
3		0.388±0.071	0.605±0.11	3.25±0.37	5.20±0.60
4			0.132±0.052	0.49±0.10	2.69±0.34
5				0.294±0.076	0.64±0.16

[a]Reference [14].

projectile electron loss is close to unity, due to the strong field of the target nucleus, partially screened by its electrons. Those authors concluded that saturation of the electron loss cross section can be explained by the constraint of the target remaining in its ground state. The same explanation can be applied here for the heaviest targets: for distant collisions, the target electron cloud has a greater overlap with the projectile electron cloud than for lighter targets. This increases the antiscreening probability, thus reducing the nonbreakup channel due to the restriction that the molecular ion cannot be excited or ionized.

In Figs. 2–6 we present the ratios of multiple to single ionization of He, Ne, Ar, Kr, and Xe, respectively, as a function of the target final charge state. In these figures, the solid circles represent the $H_2^+ + A \rightarrow H_2^+ + A^{q+}$ nondissociative channel, the up triangles are the $H_2^+ + A \rightarrow H + H^+ + A^{q+}$ breakup channel, and the inverted triangles are the $H_2^+ + A \rightarrow H^+ + H^+ + A^{q+}$ breakup channel, all from this work. Also shown in these figures are the proton data from Cavalcanti *et al.* [13] (except for He) and from Andersen *et al.* [23] (He), as open squares, and the electron data of Schram *et al.* [24] (He) and Krishnakumar and Srivastava [25] (other gases), as open diamonds. It can immediately be seen from these figures that the ratios for the nonbreakup channel are very similar to those for proton and electron projectiles for all targets and charge states, except for the double-to-single ionization ratios of Xe. It should be mentioned that this close agreement between the proton and electron ratios cannot be considered as a general feature of swift collisions with multielectron targets (see, for instance, [26] and [13]). The ratios for both breakup channels are very close and are, in all cases, larger than the nonbreakup one; the differences can reach one order of magnitude for the highest charge states.

We have attempted to make theoretical estimates for the multiple-ionization cross sections of the Ne and Ar targets in order to compare with the single- to multiple-ionization ratios measured. We have restricted our calculations to these two targets, because as will be seen later, the application of the procedure developed here can become less reliable for heavier targets. Also, there are no quantum-mechanical calculations available for the ionization probabilities of Kr and Xe by intermediate-velocity proton impact as functions of the impact parameter of the collision.

The calculations have been made in the framework of the IPM in a way similar to that presented in Refs. [12,14] for the Ne target—that is, including the contribution from time-delayed postcollisional mechanisms to the multiple ionization. However, one important modification has been made to the previous analysis in [12], which is common to both the nonbreakup and breakup channels. In that instance, we calculated the multiple-ionization cross sections in terms of the total cross sections presented by Kirchner *et al.* [27], instead of directly using calculated single-electron ionization probabilities. Here we have integrated directly the values of the ionization probabilities by proton impact, as functions of the impact parameter of the collision, for the $2s, 2p_0$, and $2p_{\pm1}$ subshells of Ne and for the $2s, 2p_0, 2p_{\pm1}, 3s, 3p_0$, and $3p_{\pm1}$ subshells of Ar [27–29]. These are the most reliable quantum-mechanical calculations for the ionization probabilities as functions of the impact parameter available. Thus, we could perform more realistic evaluations of the multiple-ionization cross sections. However, as can be seen in Figs. 7 and 8, the values of the functions $bp(b)$ for the $2p_0$ and $2p_{\pm1}$ shells for Ne are quite similar, the same occurring for the $2p_0$ and $2p_{\pm1}$ and the $3p_0$ and $3p_{\pm1}$ shells of Ar, respectively. Thus, we made the approximations $p_{2p_0}(b) \approx p_{2p_{\pm1}}(b) \approx p_{2p}(b)$ for Ne and Ar and $p_{3p_0}(b) \approx p_{3p_{\pm1}}(b) \approx p_{3p}(b)$ for Ar. Henceforth, we will employ the same notation as in [12,14].

In the case of the nonbreakup channel for the Ne target, the impact-parameter-dependent probabilities

TABLE III. Ratio multiple-to-single ionization cross sections of noble gases by H_2^+ ions: dissociative $H^+ + H^+$ channel for those projectiles aligned with the beam direction (numbers in brackets are powers of 10).

R_{q1}	He	Ne[a]	Ar	Kr	Xe
R_{21}	1.09(−2)±1.10(−3)	1.07(−1)±3.0(−3)	1.73(−1)±4.5(−3)	2.9(−1)±5.3(−3)	5.61(−1)±1.1(−2)
R_{31}		8.82(−3)±8.42(−4)	2.98(−2)±1.7(−3)	1.62(−1)±3.8(−3)	2.46(−1)±7.0(−3)
R_{41}			8.5(−3)±9.4(−4)	3.48(−2)±1.6(−3)	1.49(−1)±5.0(−3)
R_{51}				2.56(−2)±1.4(−3)	4.98(−2)±2.8(−3)

[a]Reference [14].

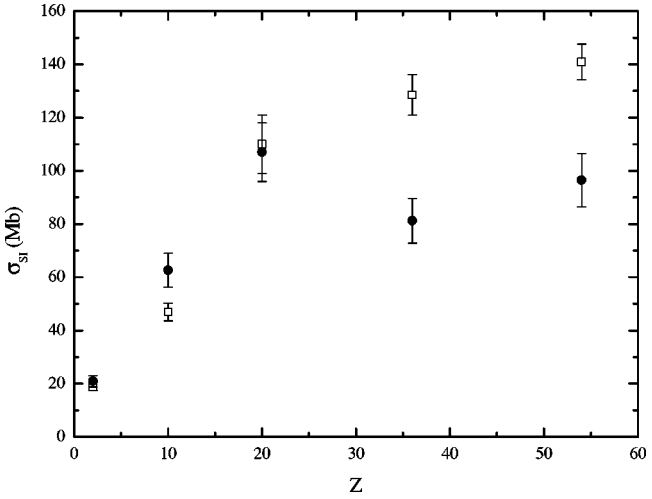

FIG. 1. Absolute single-ionization cross sections as a function of the target atomic number: solid circles, nondissociative channel, this work (1 MeV/nucleon H_2^+); open squares, Cavalcanti *et al.* [13] (2-MeV protons).

$(P_n^{(N_{1s},N_{2s},N_{2p})})_{\mathrm{NB}}(b)$ for the ionization of n electrons out of N electrons, distributed in three subshells with N_{1s}, N_{2s}, and N_{2p} electrons, can be written as

$$(P_n^{(N_{1s},N_{2s},N_{2p})})_{\mathrm{NB}}(b) = \sum_{\Sigma_i n_i + n_{\mathrm{post}} = n} \prod_{i=1}^{3} \binom{N_i}{n_i} p_i^{n_i} (1-p_i)^{N_i - n_i} \times \mathcal{P}(n_{1s}, n_{2s}, n_{2p}, n_{\mathrm{post}}). \quad (1)$$

In the above equation n_i is the number of vacancies produced by the projectile by direct ionization of the subshell i of the Ne target with probability $p_i(b)$ and $\mathcal{P}(n_{1s}, n_{2s}, n_{2p}, n_{\mathrm{post}})$ is the probability for postcollisional emission of n_{post} electrons after the creation of n_{1s}, n_{2s}, and n_{2p} vacancies in the $1s, 2s$, and $2p$ subshells of Ne, respectively.

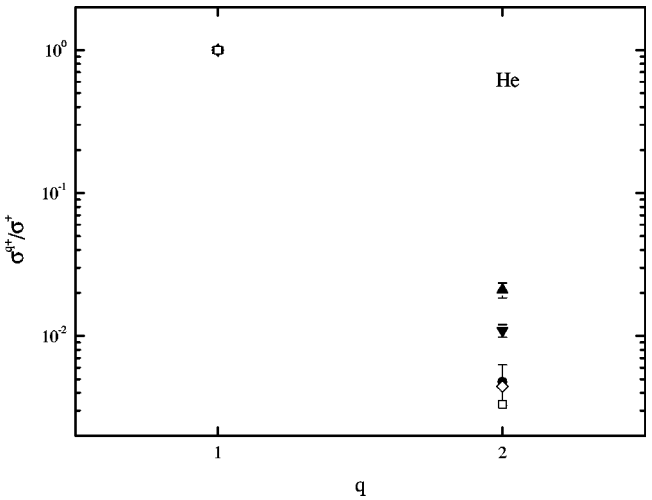

FIG. 2. Ratios of multiple- to single-ionization cross sections of He by 1 MeV/nucleon H_2^+ ions as a function of the target final charge state: circles, nondissociative channel; up triangles, $H+H^+$ dissociative channel; inverted triangles, H^++H^+ dissociative channel. Also shown are the electron data from [24] (open diamonds).

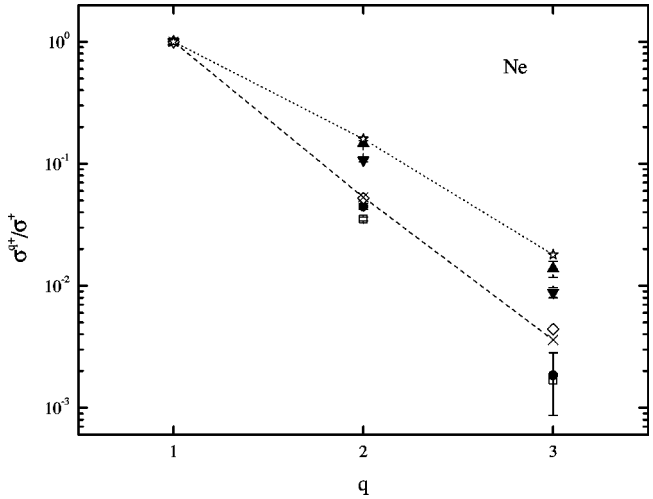

FIG. 3. Same as in Fig. 2 for the Ne target. Experiment: circles, nondissociative channel; up triangles, $H+H^+$ dissociative channel; inverted triangles, H^++H^+ dissociative channel. Also shown are the proton data from [12] (open squares) and electron data from [25] (open diamonds). Theory: crosses, nondissociative channel [see Eqs. (A9)–(A11)]; stars, dissociative channel [see Eqs. (B15)–(B17)]. The lines are just to guide the eye.

A similar expression holds for the Ar target—namely,

$$(P_n^{(N_{1s},N_{2s},N_{2p},N_{3s},N_{3p})})_{\mathrm{NB}}(b) = \sum_{\Sigma_i n_i + n_{\mathrm{post}} = n} \prod_{i=1}^{5} \binom{N_i}{n_i} p_i^{n_i} (1-p_i)^{N_i - n_i} \times \mathcal{P}(n_{1s}, n_{2s}, n_{2p}, n_{3s}, n_{3p}, n_{\mathrm{post}}), \quad (2)$$

where we have included not only the ionization probabilities of the $3s$ and $3p$ subshells of Ar, but also the probabilities $\mathcal{P}(n_{1s}, n_{2s}, n_{2p}, n_{3s}, n_{3p}, n_{\mathrm{post}})$ corresponding to the postcollisional contribution considering the $3s$ and $3p$ subshells.

In order to obtain the expressions for the multiple-ionization probabilities for the nonbreakup channel, several approximations have been made, following reasonings similar to those presented by Cavalcanti *et al.* [12]. The details of the derivations and the approximations made for the Ne and Ar targets are presented in Appendix A. There, we derive the probabilities for single, double, and triple ionizations of both Ne and Ar. We omitted the corresponding calculations for the fourfold ionization of Ar because, although the experimental result is presented here, so many approximations are needed that they would render the final result unreliable.

The multiple-ionization probabilities for the single, double, and triple ionizations of Ne and Ar for the nondissociative channel, given, respectively, by Eqs. (A9)–(A14), were used to determine the cross sections. The calculated values for the single ionization of Ne and Ar are, respectively, 57 and 133 Mb, which agree remarkably well with the measured data. The calculated double- and triple-to-single ionization cross section ratios are shown in Figs. 3 and 4 as the crosses. For the sake of comparison, the ratios obtained from the calculations of Kirchner *et al.* [28,29] for Ar, which do not take postcollisional effects fully into account, are also

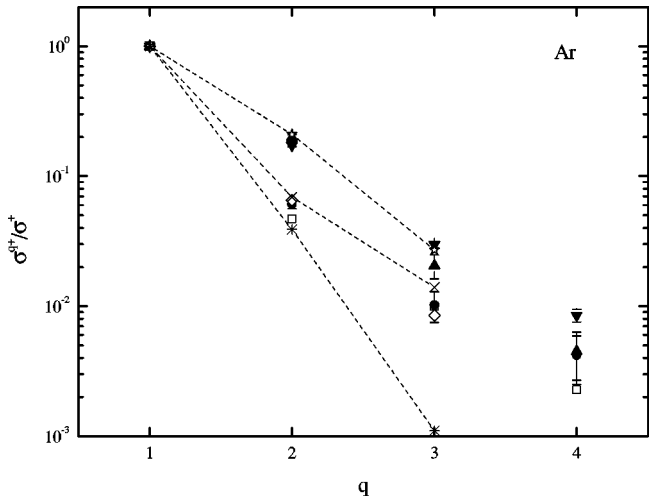

FIG. 4. Same as in Fig. 2 for the Ar target. Experiment: circles, nondissociative channel; up triangles, $H+H^+$ dissociative channel; inverted triangles, H^++H^+ dissociative channel. Also shown are the proton data from [12] (open squares) and electron data from [25] (open diamonds). Theory: crosses, nondissociative channel [see Eqs. (A12)–(A14)]; stars, dissociative channel [see Eqs. (B12), (B18), and (B19)]. Also shown as asterisks are the calculations from [28]. The lines are just to guide the eye.

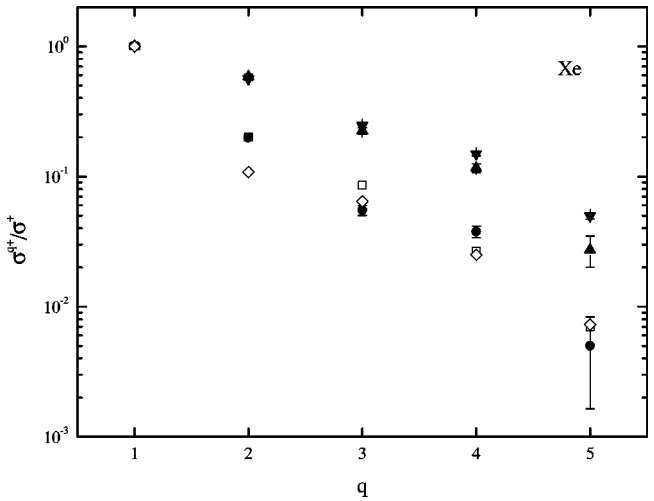

FIG. 6. Same as in Fig. 2 for the Xe target. Experiment: circles, nondissociative channel; up triangles, $H+H^+$ dissociative channel; inverted triangles, H^++H^+ dissociative channel. Also shown are the proton data from [12] (open squares) and electron data from [25] (open diamonds).

presented in Fig. 4 as asterisks (the lines are just to guide the eye). It can be seen that our results are in very good agreement with the experimental data, which show that the time-delayed postcollisional contribution is very important for the multiple target ionization. This fact has been also observed for the multiple ionization of Ne by proton impact [12].

The breakup channel, on the other hand, involves necessarily the excitation or the loss of the projectile electron, so that, in this case, we can have the concomitant excitation or ionization of both collision partners. It has been known for some time now that projectile electron loss may occur through the interaction of the projectile electron with either the target nucleus (the so-called screening process) or electrons (the antiscreening process) (see, for example, [11,30–32]).Thus, there are *two* different mechanisms contributing to the breakup channel which must be taken into account in the estimates of the total probabilities. This has been done here in a way similar to the one used above for the nonbreakup channel, with the inclusion of the antiscreening contribution, following a procedure suggested by Sant'Anna *et al.* [19]. This gives, for the Ne target,

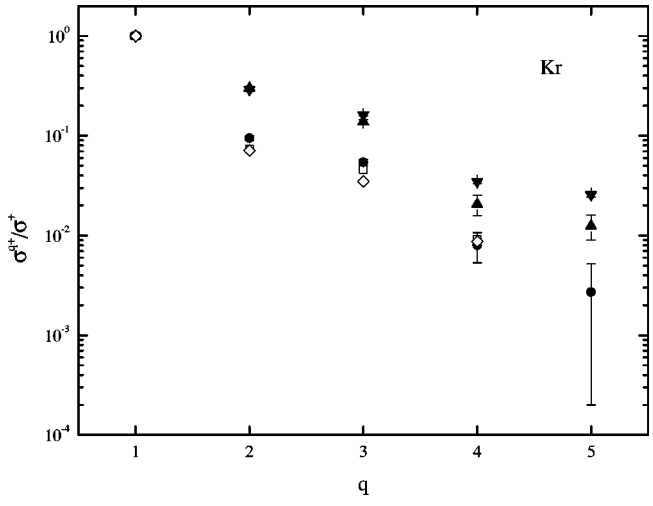

FIG. 5. Same as in Fig. 2 for the Kr target. Experiment: circles, nondissociative channel; up triangles, $H+H^+$ dissociative channel; inverted triangles, H^++H^+ dissociative channel. Also shown are the proton data from [12] (open squares) and electron data from [25] (open diamonds).

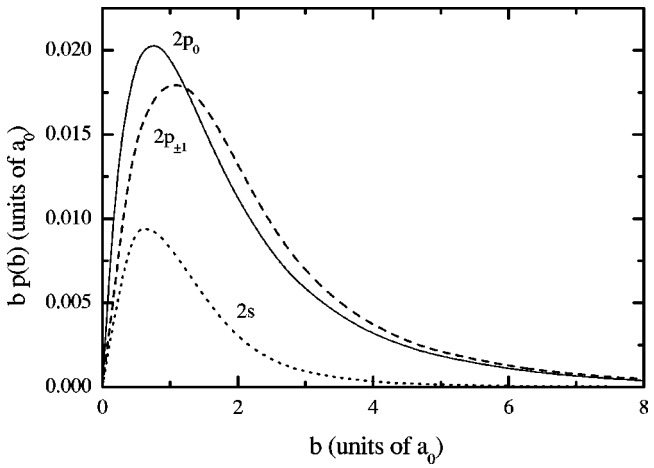

FIG. 7. Ionization probabilities times the impact parameter as a function of the impact parameter for H^+ of 1 MeV colliding with Ne: dotted line, $2s$; dashed line, $2p_{\pm1}$; solid line, $2p_0$.

$$(P_n^{(N_{1s},N_{2s},N_{2p})})_{\mathrm{B}}(b) = \sum_{\Sigma_i n_i + n_{\mathrm{post}} = n} N_i (P_{\mathrm{anti}})_i \times \binom{N_i - 1}{n_i - 1} p_i^{n_i - 1} (1 - p_i)^{N_i - n_i} \times \prod_{j \neq i} \binom{N_j}{n_j} p_j^{n_j} (1 - p_j)^{N_j - n_j} \times \mathcal{P}(n_{1s}, n_{2s}, n_{2p}, n_{\mathrm{post}}) \quad (3)$$

and, for Ar,

$$(P_n^{(N_{1s},N_{2s},N_{2p},N_{3s},N_{3p})})_{\mathrm{B}}(b) = \sum_{\Sigma_i n_i + n_{\mathrm{post}} = n} N_i (P_{\mathrm{anti}})_i \binom{N_i - 1}{n_i - 1} p_i^{n_i - 1} (1 - p_i)^{N_i - n_i} \times \prod_{j \neq i} \binom{N_j}{n_j} p_j^{n_j} (1 - p_j)^{N_j - n_j} \mathcal{P}(n_{1s}, n_{2s}, n_{2p}, n_{3s}, n_{3p}, n_{\mathrm{post}}). \quad (4)$$

In the above equations we have introduced the probability of simultaneous ionization of the projectile electron and an electron from the subshell i of the target via antiscreening, $(P_{\mathrm{anti}})_i$, and used the same notation as in Eqs. (1) and (2). Again, the details of the derivations of the multiple-ionization probabilities are presented in Appendix B.

The antiscreening probabilities, as functions of the impact parameter, which appear in Eqs. (B9)–(B14), were estimated from cross sections calculated following the procedure introduced by Montenegro and Meyerhof within the plane-wave Born approximation (PWBA) [33], using data taken from Babb and Shertzer [34] and Grémaud *et al.* [35] for the H_2^+ molecular ion. Since the antiscreening is due to the overlap of the electron clouds of the projectile and target, it ranges up to rather large values of the impact parameter of the collision. Thus, one can consider that the antiscreening probabilities do not present a strong variation with the impact parameter and can be assumed to be a step function, for simplicity [36,37]. The "cutoff" values for the impact parameters were considered as the range $\langle b \rangle^{\mathrm{AS}}$ defined by Sant'Anna *et al.* [19]. The values used here are, respectively, $\langle b \rangle_{2s}^{\mathrm{AS}} \simeq \langle b \rangle_{2p}^{\mathrm{AS}} \simeq a_0$, for Ne, and $\langle b \rangle_{2s}^{\mathrm{AS}} \simeq \langle b \rangle_{2p}^{\mathrm{AS}} \simeq a_0$ and $\langle b \rangle_{3s}^{\mathrm{AS}} \simeq \langle b \rangle_{3p}^{\mathrm{AS}} \simeq 1.75 a_0$, for Ar, where a_0 is the Bohr radius.

As pointed out in Appendix B, we have considered that only some of the target electrons (six for Ne and eight for Ar) contribute to the antiscreening, an approximation based on the findings of Montenegro *et al.* for collisions between He^+ projectiles and noble gases [32]. This assumption can be justified if one regards the antiscreening as due to the interaction of the projectile electron and a beam of quasifree equivelocity electrons (the target outer-shell, loosely bound electrons), in the projectile frame of Refs. [30–32]. An estimate of the H_2^+ ionization cross section by electrons with the same velocity as, for example, within the PWBA [33], provides a value of around 20 Mb. If one multiplies this cross section by the number of active electrons considered here for Ne and Ar, one obtains values which are consistent with the H_2^+ total destruction cross sections measured by de Castro Faria *et al.* [38].

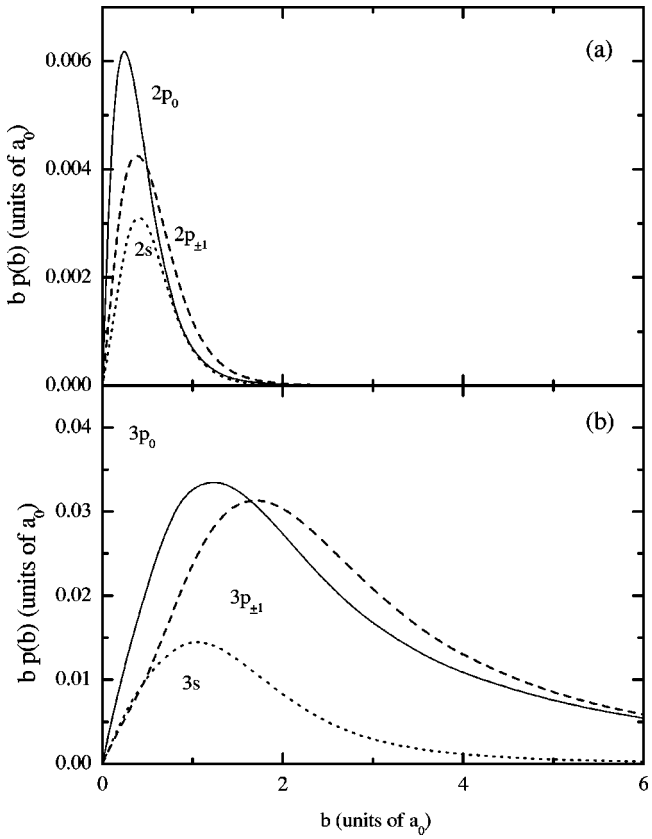

FIG. 8. Same as in Fig. 7 for Ar: (a) $2l$ subshells: dotted line, $2s$; dashed line, $2p_{\pm 1}$; solid line, $2p_0$; (b) $3l$ subshells: dotted line, $3s$; dashed line, $3p_{\pm 1}$; solid line, $3p_0$.

The multiple-ionization cross sections were obtained by integrating the product $b\,P_n(b)$ for Ne and Ar, given by Eqs. (B12) and (B15)–(B19), within the ranges specified above. The resulting multiple- to single-ionization ratios are shown in Figs. 3 and 4 as stars, with the lines to guide the eye. Again, our calculations describe the experimental data remarkably well, which is an indication that the antiscreening is the main mechanism for the ionization—with consequent dissociation—of the molecular ion projectile.

In Fig. 9 we show the absolute cross sections for the single ionization of the target, as a function of the target atomic number, for the dissociative channel $H_2^+ + A \rightarrow H^+ + H^0 + A^{q+}$. There is a remarkable suppression of the target single-ionization channel as the target atomic number increases. This suppression, which is similar to the one observed for the nondissociative channel (see Fig. 1), is in accordance with the idea of an inhibition of sequential ionization of the target electrons by the projectile fragments [14]. In fact, if the projectile molecular ion dissociates during the collision, it is not possible that a further equivalent interaction between the projectile and target electrons occurs. Any subsequent ionization of the target would be due to the interaction of its electrons with the projectile fragments, under different dynamical conditions which are now similar to the ionization by proton impact. The probability of the latter

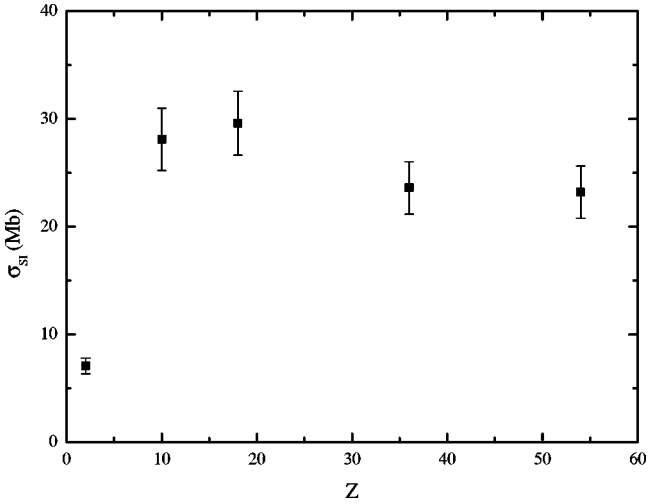

FIG. 9. Absolute single-ionization cross sections as a function of the target atomic number for the $H+H^+$ dissociative channel.

presents a dependence on the impact parameter of the collision that is quite different than that for the antiscreening, which is much broader. The convolution of the probabilities for both mechanisms gives small contributions to the total cross section for sequential ionization. This makes the postcollisional decay the main mechanism for multiple ionization, just as in the nonbreakup case.

IV. CONCLUSION

We have measured in coincidence the various final charge states of both target and projectile in collisions between 1 MeV/nucleon H_2^+ and noble gases. We have observed that, in nonbreakup collisions, the multiple- to single-ionization ratios are the same as those for protons. On the other hand, in collisions where the projectile molecular ion breaks up, we have observed that the multiple- to single-ionization ratios (i) are approximately equal for both the nonaligned $H+H^+$ and the aligned H^++H^+ dissociative channels and (ii) are systematically larger than those for the nonbreakup channel. The first of these observations leads to the important conclusion that the orientation of the axis of the projectile molecular ion relative to the incident direction is not relevant to the multiple-ionization ratios of the target.

We have developed equations for the probabilities of multiple ionization of Ne and Ar which take into account time-delayed postcollisional effects, within the framework of the IPM. These equations may become quite cumbersome as the final charge state and/or the atomic number of the target increases. We have employed postcollisional probabilities obtained from photoionization experimental data, which do not include the influence of postcollisional interactions on the decay as pointed out in [12]. Both these features have made us introduce several approximations in our calculations. In spite of these limitations, not only the absolute single-ionization cross sections but also the multiple-to-single ionization ratios for the nondissociative channel are in remarkably good agreement with the experiment, thus showing that the previous findings for Ne [12,14] are also valid for Ar. This means that, when the projectile remains unchanged during the collision, time-delayed postcollisional mechanisms effectively contribute to the target multiple ionization. Unfortunately, the lack of reliable quantum-mechanical calculations for the ionization probabilities of heavier targets by protons still prevent the conclusion that this is a general feature of multiple ionization. However, our calculations enabled us to verify the relative importance of the various pathways leading to target multiple ionization. In fact, we could determine quantitatively that the higher the target final charge state, the greater the relative contribution of postcollisional mechanisms. These are responsible, for example, for approximately 50% and for more than 90% of the triple-ionization cross sections of Ne and Ar for the nonbreakup channel, respectively.

For the dissociative channels, we have included in our calculations the contribution due to the antiscreening mechanism to the simultaneous ionization of the projectile molecular ion and target atom. Again, the agreement with the experimental results is very good. Since the antiscreening is an effect that does not appear in the nondissociative channel, its inclusion explains why the multiple- to single-ionization ratios are larger for the breakup than for the nonbreakup channels.

The fact that both the absolute single-ionization cross sections for the nondissociative and the $H+H^+$ exit channels present a strong saturation as the target atomic number increases, together with the importance of time-delayed postcollisional decay mechanisms to the target multiple ionization, indicates that the contribution of further interactions between the projectile fragments—after its breakup—and the target electrons is strongly inhibited.

ACKNOWLEDGMENTS

The authors wish to thank Dr. T. Kirchner for providing the ionization probabilities for multiple ionization of Ne and Ar by protons. This work was supported in part by the Brazilian agencies CNPq, FINEP, CAPES, FAPERJ, and MCT (PRONEX), by the Volkswagen Stiftung (Germany), by the U.K. EPSRC, and by the Department of Education, Northern Ireland.

APPENDIX A: MULTIPLE-IONIZATION PROBABILITIES FOR THE NONBREAKUP CHANNEL

To obtain the equations for the multiple-ionization probabilities from Eqs. (1) and (2) for the nonbreakup channel, we have considered several approximations. First of all, since the 1*s* ionization probability is much smaller than the ones for the other subshells of both targets, we neglected the terms involving p_{1s} in the above equations. Second, it can be seen from Figs. 7 and 8 that, for high velocities, all the probabilities $p(b)$ have values much smaller than 1 for all impact parameters, so that we can also make the approximation $(1-p_i)\approx 1$. Also, we considered that the probabilities of time-delayed postcollisional emission of electrons after the ionization of the outermost subshell of the target are negligible—that is, $\mathcal{P}(0,0,n_{2p},n_{\mathrm{post}})$ (for Ne) $\approx\mathcal{P}(0,0,0,0,n_{3p},n_{\mathrm{post}})$ (for Ar) ≈ 0, with $n_{2p},n_{3p},n_{\mathrm{post}}\neq 0$. Thus, one can write the single-, double-, and triple-ionization

probabilities of Ne for the nonbreakup channel, respectively, including time-delayed postcollisional contributions, approximately as

$$(P_{\mathrm{SI}}^{\mathrm{Ne}})_{\mathrm{NB}} \simeq 2p_{2s}\mathcal{P}(0,1,0,0) + 6p_{2p}\mathcal{P}(0,0,1,0), \tag{A1}$$

$$(P_{\mathrm{DI}}^{\mathrm{Ne}})_{\mathrm{NB}} \simeq p_{2s}^2\mathcal{P}(0,2,0,0) + 2p_{2s}\mathcal{P}(0,1,0,1) + 12p_{2s}p_{2p}\mathcal{P}(0,1,1,0) + 15p_{2p}^2\mathcal{P}(0,0,2,0), \tag{A2}$$

and

$$\begin{aligned}(P_{\mathrm{TI}}^{\mathrm{Ne}})_{\mathrm{NB}} \simeq{}& 20p_{2p}^3\mathcal{P}(0,0,3,0) + 30p_{2s}p_{2p}^2\mathcal{P}(0,1,2,0) + 6p_{2s}^2p_{2p}\mathcal{P}(0,2,1,0) + 12p_{2s}p_{2p}\mathcal{P}(0,1,1,1) + p_{2s}^2\mathcal{P}(0,2,0,1)\\ &+ 2p_{2s}\mathcal{P}(0,1,0,2).\end{aligned} \tag{A3}$$

The corresponding equations for Ar are

$$(P_{\mathrm{SI}}^{\mathrm{Ar}})_{\mathrm{NB}} \simeq 2p_{2s}\mathcal{P}(0,1,0,0,0,0) + 6p_{2p}\mathcal{P}(0,0,1,0,0,0) + 2p_{3s}\mathcal{P}(0,0,0,1,0,0) + 6p_{2p}\mathcal{P}(0,0,0,0,1,0), \tag{A4}$$

$$\begin{aligned}(P_{\mathrm{DI}}^{\mathrm{Ar}})_{\mathrm{NB}} \simeq{}& p_{2s}^2\mathcal{P}(0,2,0,0,0,0) + 15p_{2p}^2\mathcal{P}(0,0,2,0,0,0) + 12p_{2s}p_{2p}\mathcal{P}(0,1,1,0,0,0) + 2p_{2s}\mathcal{P}(0,1,0,0,0,1) + 6p_{2p}\mathcal{P}(0,0,1,0,0,1)\\ &+ 4p_{2s}p_{3s}\mathcal{P}(0,1,0,1,0,0) + 12p_{2s}p_{3p}\mathcal{P}(0,1,0,0,1,0) + 12p_{2p}p_{3s}\mathcal{P}(0,0,1,1,0,0) + 36p_{2p}p_{3p}\mathcal{P}(0,0,1,0,1,0)\\ &+ p_{3s}^2\mathcal{P}(0,0,0,2,0,0) + 15p_{3p}^2\mathcal{P}(0,0,0,0,2,0) + 12p_{3s}p_{3p}\mathcal{P}(0,0,0,1,1,0) + 2p_{3s}\mathcal{P}(0,0,0,1,0,1),\end{aligned} \tag{A5}$$

and

$$\begin{aligned}(P_{\mathrm{TI}}^{\mathrm{Ar}})_{\mathrm{NB}} \simeq{}& 6p_{2s}^2p_{2p}\mathcal{P}(0,2,1,0,0,0) + 30p_{2s}p_{2p}^2\mathcal{P}(0,1,2,0,0,0) + p_{2s}^2\mathcal{P}(0,2,0,0,0,1) + 12p_{2s}p_{2p}\mathcal{P}(0,1,1,0,0,1)\\ &+ 2p_{2s}\mathcal{P}(0,1,0,0,0,2) + 20p_{2p}^3\mathcal{P}(0,0,3,0,0,0) + 15p_{2p}^2\mathcal{P}(0,0,2,0,0,1) + 6p_{2p}\mathcal{P}(0,0,1,0,0,2) + 2p_{2s}^2p_{3s}\mathcal{P}(0,2,0,1,0,0)\\ &+ 2p_{2s}p_{3s}^2\mathcal{P}(0,1,0,2,0,0) + 6p_{2s}^2p_{3p}\mathcal{P}(0,2,0,0,1,0) + 30p_{2s}p_{3p}^2\mathcal{P}(0,1,0,0,2,0) + 4p_{2s}p_{3s}\mathcal{P}(0,1,0,1,0,1)\\ &+ 12p_{2s}p_{3p}\mathcal{P}(0,1,0,0,1,1) + 30p_{2p}^2p_{3s}\mathcal{P}(0,0,2,1,0,0) + 90p_{2p}^2p_{3p}\mathcal{P}(0,0,2,0,1,0) + 6p_{2p}p_{3s}^2\mathcal{P}(0,0,1,2,0,0)\\ &+ 90p_{2p}p_{3p}^2\mathcal{P}(0,0,1,0,2,0) + 24p_{2s}p_{2p}p_{3s}\mathcal{P}(0,1,1,1,0,0) + 72p_{2s}p_{2p}p_{3p}\mathcal{P}(0,1,1,0,1,0) + 24p_{2s}p_{3s}p_{3p}\mathcal{P}(0,1,0,1,1,0)\\ &+ 72p_{2p}p_{3s}p_{3p}\mathcal{P}(0,0,1,1,1,0) + 12p_{2p}p_{3s}\mathcal{P}(0,0,1,1,0,1) + 36p_{2p}p_{3p}\mathcal{P}(0,0,1,0,1,1) + 6p_{3s}^2p_{3p}\mathcal{P}(0,0,0,2,1,0)\\ &+ 30p_{3s}p_{3p}^2\mathcal{P}(0,0,0,1,2,0) + p_{3s}^2\mathcal{P}(0,0,0,2,0,1) + 12p_{3s}p_{3p}\mathcal{P}(0,0,0,1,1,1) + 2p_{3s}\mathcal{P}(0,0,0,1,0,2)\\ &+ 20p_{3p}^3\mathcal{P}(0,0,0,0,3,0).\end{aligned} \tag{A6}$$

For the double- and triple-ionization probabilities of Ar, a further approximation has been made. From the values of the subshell ionization probabilities (see Fig. 8), one can see that $p_{2s}, p_{2p} \ll p_{3s}, p_{3p}$, so that we considered $p_{2l}^2, p_{2l}p_{3l} \ll p_{3l}^2$ and $p_{2l}^3, p_{2l}^2p_{3l}, p_{2l}p_{3l}^2 \ll p_{3l}^3$ in Eqs. (A5) and (A6). However, we kept terms containing p_{2s} and p_{2p} in both equations and p_{2s}^2 and p_{2p}^2 in Eq. (A6). Thus, Eqs. (A5) and (A6) become, respectively,

$$\begin{aligned}(P_{\mathrm{DI}}^{\mathrm{Ar}})_{\mathrm{NB}} \simeq{}& 2p_{2s}\mathcal{P}(0,1,0,0,0,1) + 6p_{2p}\mathcal{P}(0,0,1,0,0,1) + p_{3s}^2\mathcal{P}(0,0,0,2,0,0) + 15p_{3p}^2\mathcal{P}(0,0,0,0,2,0) + 12p_{3s}p_{3p}\mathcal{P}(0,0,0,1,1,0)\\ &+ 2p_{3s}\mathcal{P}(0,0,0,1,0,1)\end{aligned} \tag{A7}$$

and

$$\begin{aligned}(P_{\mathrm{TI}}^{\mathrm{Ar}})_{\mathrm{NB}} \simeq{}& p_{2s}^2\mathcal{P}(0,2,0,0,0,1) + 12p_{2s}p_{2p}\mathcal{P}(0,1,1,0,0,1) + 2p_{2s}\mathcal{P}(0,1,0,0,0,2) + 15p_{2p}^2\mathcal{P}(0,0,2,0,0,1) + 6p_{2p}\mathcal{P}(0,0,1,0,0,2)\\ &+ 4p_{2s}p_{3s}\mathcal{P}(0,1,0,1,0,1) + 12p_{2s}p_{3p}\mathcal{P}(0,1,0,0,1,1) + 12p_{2p}p_{3s}\mathcal{P}(0,0,1,1,0,1) + 36p_{2p}p_{3p}\mathcal{P}(0,0,1,0,1,1)\\ &+ 6p_{3s}^2p_{3p}\mathcal{P}(0,0,0,2,1,0) + 30p_{3s}p_{3p}^2\mathcal{P}(0,0,0,1,2,0) + p_{3s}^2\mathcal{P}(0,0,0,2,0,1) + 12p_{3s}p_{3p}\mathcal{P}(0,0,0,1,1,1)\\ &+ 2p_{3s}\mathcal{P}(0,0,0,1,0,2) + 20p_{3p}^3\mathcal{P}(0,0,0,0,3,0).\end{aligned} \tag{A8}$$

The values of the probabilities for postcollisional electron emission, $\mathcal{P}(n_{1s}, n_{2s}, n_{2p}, n_{\mathrm{post}})$ and $\mathcal{P}(n_{1s}, n_{2s}, n_{2p}, n_{3s}, n_{3p}, n_{\mathrm{post}})$ for Ne and Ar, respectively, were obtained as follows. First, we used the experimental postcollisional decay probabilities for Ne and Ar published by Carlson *et al.* [39], obtained from photoionization. Of course, the postcollisional probabilities obtained from photoionization do not include the influence of postcollisional *interactions* on the decay. However, this influence is expected to be small at high projectile velocities. Thus, for Ne we used

$$\mathcal{P}(0,1,0,0) = 0.873, \mathcal{P}(0,1,0,0) = 0.119, \text{and } \mathcal{P}(0,1,0,0) = 0.008$$

and, for

$$\text{Ar, } \mathcal{P}(0,0,1,0,0,0) = \mathcal{P}(0,1,0,0,0,0) = 0, \mathcal{P}(0,0,0,1,0,0) = 0.855, \mathcal{P}(0,0,0,1,0,1) = 0.135, \mathcal{P}(0,0,1,0,0,1)$$
$$= 0.74, \mathcal{P}(0,1,0,0,0,1) = 0.02, \mathcal{P}(0,1,0,0,0,2) = 0.72, \text{and } \mathcal{P}(0,0,1,0,0,2) = 0.24$$

[39].

Second, as mentioned above, we considered that the probabilities of time-delayed postcollisional emission of electrons after ionization of the outermost subshell of the target to be negligible, which means that $\mathcal{P}(0,0,n_{2p},0) = \mathcal{P}(0,0,0,0,n_{3p},0) \approx 1$, except for $\mathcal{P}(0,0,0,0,1,0)$, which was taken as 0.978, according to the calculations of El-Shemi *et al.* [40].

Finally, the other postcollisional probabilities which appear in Eqs. (A2), (A3), (A7), and (A8) were estimated following a procedure which considers that the target electrons are independent. Some examples are, for Ne,

$$\mathcal{P}(0,1,1,0) \simeq 1 - \tfrac{5}{6}[1 - \mathcal{P}(0,1,0,0)] \simeq 0.894,$$

$$\mathcal{P}(0,2,0,0) \simeq [\mathcal{P}(0,1,0,0)]^2 \simeq 0.762,$$

$$\mathcal{P}(0,1,1,1) \simeq 2[\mathcal{P}(0,2,0,0)\mathcal{P}(0,1,0,1)] \simeq 0.181$$

and, for Ar,

$$\mathcal{P}(0,0,0,1,1,0) \simeq 1 - \tfrac{5}{6}[1 - \mathcal{P}(0,0,0,1,0,0)] \simeq 0.879,$$

$$\mathcal{P}(0,0,0,2,0,0) \simeq [\mathcal{P}(0,0,0,1,0,0)]^2 \simeq 0.731,$$

$$\mathcal{P}(0,1,0,1,0,1) \simeq 2[\mathcal{P}(0,0,0,1,0,0)\mathcal{P}(0,1,0,0,0,1)] \simeq 0.0342.$$

Thus, one can write the single-, double-, and triple-ionization probabilities for Ne, respectively, as

$$(P_{\mathrm{SI}}^{\mathrm{Ne}})_{\mathrm{NB}} \simeq 1.75p_{2s} + 6p_{2p}, \tag{A9}$$

$$(P_{\mathrm{DI}}^{\mathrm{Ne}})_{\mathrm{NB}} \simeq 0.762p_{2s}^2 + 0.238p_{2s} + 10.7p_{2s}p_{2p} + 15p_{2p}^2, \tag{A10}$$

and

$$(P_{\mathrm{TI}}^{\mathrm{Ne}})_{\mathrm{NB}} \simeq 20p_{2p}^3 + 27.45p_{2s}p_{2p}^2 + 4.81p_{2s}^2p_{2p} + 1.2p_{2s}p_{2p} + 0.181p_{2s}^2 + 0.016p_{2s}. \tag{A11}$$

The corresponding equations for Ar are, respectively,

$$(P_{\mathrm{SI}}^{\mathrm{Ar}})_{\mathrm{NB}} \simeq 1.71p_{3s} + 5.87p_{2p}, \tag{A12}$$

$$(P_{\mathrm{DI}}^{\mathrm{Ar}})_{\mathrm{NB}} \simeq 0.04p_{2s} + 4.44p_{2p} + 0.731p_{3s}^2 + 14.34p_{3p}^2 + 10.55p_{3s}p_{3p} + 0.27p_{3s}, \tag{A13}$$

and

$$(P_{\mathrm{TI}}^{\mathrm{Ar}})_{\mathrm{NB}} \simeq 1.44p_{2s} + 1.44p_{2p} + 0.136p_{2s}p_{3s} + 0.204p_{2s}p_{3p} + 22.21p_{2p}p_{3p} + 4.66p_{3s}^2p_{3p} + 27.09p_{3s}p_{3p}^2 + 0.197p_{3s}^2 + 1.36p_{3s}p_{3p}$$
$$+ 0.02p_{3s} + 18.7p_{3p}^3. \tag{A14}$$

APPENDIX B: MULTIPLE-IONIZATION PROBABILITIES FOR THE BREAKUP CHANNEL

Making the same approximations as stated in the first paragraph of Appendix A, one can write Eqs. (3) and (4), for the multiple ionization of Ne and Ar with the breakup of the projectile molecular ion, respectively, as

$$(P_n^{(N_{1s},N_{2s},N_{2p})})_{\mathrm{B}}^{Ne} \simeq \sum_{n_{2s}+n_{2p}+n_{\mathrm{post}}=n} [n_{2s}(P_{\mathrm{anti}})_{2s}p_{2p} + n_{2p}(P_{\mathrm{anti}})_{2p}p_{2s}]\binom{2}{n_{2s}} p_{2s}^{n_{2s}-1}\binom{6}{n_{2p}} p_{2p}^{n_{2p}-1}\mathcal{P}(n_{1s},n_{2s},n_{2p},n_{\mathrm{post}}) \tag{B1}$$

and

$$(P_n^{(N_{1s},N_{2s},N_{2p},N_{3s},N_{3p})})_{\mathrm{B}}^{Ar} \simeq \sum_{n_{2s}+n_{2p}+n_{3s}+n_{3p}+n_{\mathrm{post}}=n} [n_{2s}(P_{\mathrm{anti}})_{2s}p_{2p}p_{3s}p_{3p} + n_{2p}(P_{\mathrm{anti}})_{2p}p_{2s}p_{3s}p_{3p} + n_{3s}(P_{\mathrm{anti}})_{3s}p_{2s}p_{2p}p_{3p} + n_{3p}(P_{\mathrm{anti}})_{3p}p_{2s}p_{2p}p_{3s}]\binom{2}{n_{2s}}p_{2s}^{n_{2s}-1}\binom{6}{n_{2p}}p_{2p}^{n_{2p}-1}\binom{2}{n_{3s}}p_{3s}^{n_{3s}-1}\binom{6}{n_{3p}}p_{3p}^{n_{3p}-1}\mathcal{P}(n_{1s},n_{2s},n_{2p},n_{3s},n_{3p},n_{\mathrm{post}}). \tag{B2}$$

From the above equations, one can write the probability for single, double, and triple ionization of Ne and Ar, respectively, as

$$(P_{\mathrm{SI}}^{\mathrm{Ne}})_{\mathrm{B}} \simeq 2(P_{\mathrm{anti}})_{2s}\mathcal{P}(0,1,0,0) + 6(P_{\mathrm{anti}})_{2p}\mathcal{P}(0,0,1,0), \tag{B3}$$

$$(P_{\mathrm{DI}}^{\mathrm{Ne}})_{\mathrm{B}} \simeq 2(P_{\mathrm{anti}})_{2s}\mathcal{P}(0,1,0,1) + 2(P_{\mathrm{anti}})_{2s}p_{2s}\mathcal{P}(0,2,0,0) + 30(P_{\mathrm{anti}})_{2p}p_{2p}\mathcal{P}(0,0,2,0) + 12[(P_{\mathrm{anti}})_{2s}p_{2p} + (P_{\mathrm{anti}})_{2p}p_{2s}]\mathcal{P}(0,1,1,0), \tag{B4}$$

$$(P_{\mathrm{TI}}^{\mathrm{Ne}})_{\mathrm{B}} \simeq 2(P_{\mathrm{anti}})_{2s}\mathcal{P}(0,1,0,2) + 6[2(P_{\mathrm{anti}})_{2s}p_{2p} + (P_{\mathrm{anti}})_{2p}p_{2s}]p_{2s}\mathcal{P}(0,2,1,0) + 2(P_{\mathrm{anti}})_{2s}p_{2s}\mathcal{P}(0,2,0,1) + 30[(P_{\mathrm{anti}})_{2s}p_{2p} + 2(P_{\mathrm{anti}})_{2p}p_{2s}]p_{2p}\mathcal{P}(0,1,2,0) + 12[(P_{\mathrm{anti}})_{2s}p_{2p} + (P_{\mathrm{anti}})_{2p}p_{2s}]\mathcal{P}(0,1,1,1) + 60(P_{\mathrm{anti}})_{2p}p_{2p}^2\mathcal{P}(0,0,3,0), \tag{B5}$$

$$(P_{\mathrm{SI}}^{\mathrm{Ar}})_{\mathrm{B}} \simeq 2(P_{\mathrm{anti}})_{3s}\mathcal{P}(0,0,0,1,0,0) + 6(P_{\mathrm{anti}})_{3p}\mathcal{P}(0,0,0,0,1,0), \tag{B6}$$

$$(P_{\mathrm{DI}}^{\mathrm{Ar}})_{\mathrm{B}} \simeq 2(P_{\mathrm{anti}})_{3s}\mathcal{P}(0,0,0,1,0,1) + 2(P_{\mathrm{anti}})_{3s}p_{3s}\mathcal{P}(0,0,0,2,0,0) + 30(P_{\mathrm{anti}})_{3p}p_{3p}\mathcal{P}(0,0,0,0,2,0) + 12[(P_{\mathrm{anti}})_{3s}p_{3p} + (P_{\mathrm{anti}})_{3p}p_{3s}]\mathcal{P}(0,0,0,1,1,0) + 6(P_{\mathrm{anti}})_{2p}\mathcal{P}(0,0,1,0,0,1) + 2(P_{\mathrm{anti}})_{2s}\mathcal{P}(0,1,0,0,0,1), \tag{B7}$$

and

$$\begin{aligned}(P_{\mathrm{TI}}^{\mathrm{Ar}})_{\mathrm{B}} \simeq\ & 2\,(P_{\mathrm{anti}})_{3s}\,\mathcal{P}(0,0,0,1,0,2) + 6[2\,(P_{\mathrm{anti}})_{3s}\,p_{3p} + (P_{\mathrm{anti}})_{3p}\,p_{3s}]p_{3s}\,\mathcal{P}(0,0,0,2,1,0) + 2(P_{\mathrm{anti}})_{3s}p_{3s}\mathcal{P}(0,0,0,2,0,1)\\ & + 30[(P_{\mathrm{anti}})_{3s}p_{3p} + 2(P_{\mathrm{anti}})_{3p}p_{3s}]p_{3p}\mathcal{P}(0,0,0,1,2,0) + 12[(P_{\mathrm{anti}})_{3s}p_{3p} + (P_{\mathrm{anti}})_{3p}p_{3s}]\mathcal{P}(0,0,0,1,1,1)\\ & + 60(P_{\mathrm{anti}})_{3p}p_{3p}^2\mathcal{P}(0,0,0,0,3,0) + 2(P_{\mathrm{anti}})_{2s}\mathcal{P}(0,1,0,0,0,2) + 4[(P_{\mathrm{anti}})_{2s}p_{3s} + (P_{\mathrm{anti}})_{3s}p_{2s}]\mathcal{P}(0,1,0,1,0,1)\\ & + 6(P_{\mathrm{anti}})_{2p}\mathcal{P}(0,0,1,0,0,2) + 12[(P_{\mathrm{anti}})_{2s}p_{3p} + (P_{\mathrm{anti}})_{3p}p_{2s}]\mathcal{P}(0,1,0,0,1,1) + 36[(P_{\mathrm{anti}})_{2p}p_{3p}\\ & + (P_{\mathrm{anti}})_{3p}p_{2p}]\mathcal{P}(0,0,1,0,1,1).\end{aligned} \tag{B8}$$

In the above equations, we have already omitted the terms containing vanishing postcollisional probabilities. Substituting now the values of the nonvanishing postcollisional probabilities, Eqs. (B3)–(B8) become, respectively,

$$(P_{\mathrm{SI}}^{\mathrm{Ne}})_{\mathrm{B}} \simeq 1.75(P_{\mathrm{anti}})_{2s} + 6(P_{\mathrm{anti}})_{2p}, \tag{B9}$$

$$(P_{\mathrm{DI}}^{\mathrm{Ne}})_{\mathrm{B}} \simeq (P_{\mathrm{anti}})_{2s}(10.73p_{2p} + 1.52p_{2s} + 0.238) + (P_{\mathrm{anti}})_{2p}(30p_{2p} + 10.73p_{2s}), \tag{B10}$$

$$(P_{\mathrm{TI}}^{\mathrm{Ne}})_{\mathrm{B}} \simeq (P_{\mathrm{anti}})_{2s}(27.45p_{2p}^2 + 9.14p_{2s}p_{2p} + 0.36p_{2s} + 1.19p_{2p} + 0.016) + (P_{\mathrm{anti}})_{2p}(60p_{2p}^2 + 54.9p_{2s}p_{2p} + 4.57p_{2s}^2 + 1.19p_{2s}), \tag{B11}$$

$$(P_{\mathrm{SI}}^{\mathrm{Ar}})_{\mathrm{B}} \simeq 1.71(P_{\mathrm{anti}})_{3s} + 5.87(P_{\mathrm{anti}})_{3p}, \tag{B12}$$

$$(P_{\mathrm{DI}}^{\mathrm{Ar}})_{\mathrm{B}} \simeq (P_{\mathrm{anti}})_{3s}(1.46p_{3s} + 10.55p_{3p} + 0.27) + (P_{\mathrm{anti}})_{3p}(28.68p_{3p} + 10.55p_{3s}) + 4.44(P_{\mathrm{anti}})_{2p} + 0.04(P_{\mathrm{anti}})_{2s}, \tag{B13}$$

and

$$(P_{\mathrm{TI}}^{\mathrm{Ar}})_{\mathrm{B}} \simeq (P_{\mathrm{anti}})_{3s}(27.1p_{3p}^2 + 1.36p_{3p} + 0.39p_{3s} + 9.31p_{3s}p_{3p} + 0.14p_{2s} + 0.02) + (P_{\mathrm{anti}})_{3p}(56.1p_{3p}^2 + 4.66p_{3s}^2 + 1.36p_{3s} + 54.2p_{3s}p_{3p} + 22.2p_{2p} + 0.2p_{2s}) + (P_{\mathrm{anti}})_{2s}(0.14p_{3s} + 0.2p_{3p} + 1.44) + (P_{\mathrm{anti}})_{2p}(22.2p_{3p} + 1.44). \tag{B14}$$

The antiscreening probabilities which appear in Eqs. (B9)–(B14) are, from the target point of view, probabilities *per electron*. Based on results from Montenegro *et al.* [32], we considered the target electrons *active* for the antiscreening to be the outermost ones for both Ne and Ar. This leads to the further approximations $(P_{\mathrm{anti}})_{2s} \ll (P_{\mathrm{anti}})_{2p}$ for Ne and $(P_{\mathrm{anti}})_{2l} \ll (P_{\mathrm{anti}})_{3l}$ for Ar, so that Eqs. (B9)–(B11), (B13), and (B14) become, respectively,

$$(P_{\mathrm{SI}}^{\mathrm{Ne}})_{\mathrm{B}} \simeq 6(P_{\mathrm{anti}})_{2p}, \tag{B15}$$

$$(P_{\mathrm{DI}}^{\mathrm{Ne}})_{\mathrm{B}} \simeq (P_{\mathrm{anti}})_{2p}(30p_{2p} + 10.73p_{2s}), \tag{B16}$$

$$(P_{\mathrm{TI}}^{\mathrm{Ne}})_{\mathrm{B}} \simeq (P_{\mathrm{anti}})_{2p}(60p_{2p}^2 + 54.9p_{2s}p_{2p} + 4.57p_{2s}^2 + 1.19p_{2s}), \tag{B17}$$

$$(P_{\mathrm{DI}}^{\mathrm{Ar}})_{\mathrm{B}} \simeq (P_{\mathrm{anti}})_{3s}(1.46p_{3s} + 10.55p_{3p} + 0.27) + (P_{\mathrm{anti}})_{3p}(28.68p_{3p} + 10.55p_{3s}), \tag{B18}$$

and

$$(P_{\mathrm{TI}}^{\mathrm{Ar}})_{\mathrm{B}} \simeq (P_{\mathrm{anti}})_{3s}(27.1p_{3p}^2 + 1.36p_{3p} + 0.39p_{3s} + 9.31p_{3s}p_{3p} + 0.14p_{2s} + 0.02) + (P_{\mathrm{anti}})_{3p}(56.1p_{3p}^2 + 4.66p_{3s}^2 + 1.36p_{3s} + 54.2p_{3s}p_{3p} + 22.2p_{2p} + 0.2p_{2s}). \tag{B19}$$

[1] T. F. Tuan and E. Gerjuoy, Phys. Rev. **117**, 756 (1960).
[2] S. L. Varghese, C. L. Cocke, S. Cheng, E. Y. Kamber, and V. Frohne, Nucl. Instrum. Methods Phys. Res. B **40/41**, 266 (1989).
[3] A. K. Edwards, R. M. Wood, M. A. Mangan, and R. L. Ezell, Phys. Rev. A **46**, 6970 (1992).
[4] S. Cheng, C. L. Cocke, V. Frohne, E. Y. Kamber, J. H. McGuire, and Y. Wang, Phys. Rev. A **47**, 3923 (1993).
[5] U. Werner, N. M. Kabachnik, V. N. Kondratyev, and H. O. Lutz, Phys. Rev. Lett. **79**, 1662 (1997).
[6] N. Stolterfoht *et al.*, Phys. Rev. Lett. **87**, 023201 (2001).
[7] I. Reiser and C. L. Cocke, Nucl. Instrum. Methods Phys. Res. B **205**, 614 (2003).
[8] I. Reiser, C. L. Cocke, and H. Bräuning, Phys. Rev. A **67**, 062718 (2003).
[9] W. E. Meyerhof, H.-P. Hülskötter, Q. Dai, J. H. McGuire, and Y. D. Wang, Phys. Rev. A **43**, 5907 (1991).
[10] M. M. Sant'Anna, W. S. Melo, A. C. F. Santos, G. M. Sigaud, E. C. Montenegro, M. B. Shah, and W. E. Meyerhof, Phys. Rev. A **58**, 1204 (1998).
[11] E. C. Montenegro, G. M. Sigaud, and W. E. Meyerhof, Phys. Rev. A **45**, 1575 (1992).
[12] E. G. Cavalcanti, G. M. Sigaud, E. C. Montenegro, M. M. Sant'Anna, and H. Schmidt-Böcking, J. Phys. B **35**, 3937 (2002).
[13] E. G. Cavalcanti, G. M. Sigaud, E. C. Montenegro, and H. Schmidt-Böcking, J. Phys. B **36**, 3087 (2003).
[14] M. M. Sant'Anna, H. Luna, A. C. F. Santos, C. McGrath, M. B. Shah, E. G. Cavalcanti, G. M. Sigaud, and E. C. Montenegro, Phys. Rev. A **68**, 042707 (2003).
[15] M. M. Sant'Anna, W. S. Melo, A. C. F. Santos, G. M. Sigaud, and E. C. Montenegro, Nucl. Instrum. Methods Phys. Res. B **99**, 46 (1995).
[16] A. E. Voitkiv, G. M. Sigaud, and E. C. Montenegro, Phys. Rev. A **59**, 2794 (1999).
[17] W. S. Melo, M. M. Sant'Anna, A. C. F. Santos, G. M. Sigaud, and E. C. Montenegro, Phys. Rev. A **60**, 1124 (1999).
[18] A. C. F. Santos, W. S. Melo, M. M. Sant'Anna, G. M. Sigaud, and E. C. Montenegro, Phys. Rev. A **63**, 062717 (2001).
[19] M. M. Sant'Anna, H. Luna, A. C. F. Santos, C. McGrath, M. B. Shah, E. G. Cavalcanti, G. M. Sigaud, and E. C. Montenegro, Phys. Scr. (to be published).
[20] E. P. Kanter, P. J. Cooney, D. S. Gemmell, K. O. Groeneveld, W. J. Ratkowski, Z. Vager, and B. J. Zabransky, Phys. Rev. A **20**, 834 (1979).
[21] D. Calabrese, L. M. Wiese, O. Yenen, and D. H. Jaecks, Phys. Rev. A **50**, 4899 (1994).
[22] A. C. F. Santos, W. S. Melo, M. M. Sant'Anna, G. M. Sigaud, and E. C. Montenegro, Rev. Sci. Instrum. **73**, 2369 (2002).
[23] L. H. Andersen, P. Hvelplund, H. Knudsen, S. P. Møller, A. H. Sørensen, K. Elsener, K.-G. Rensfeld, and E. Uggerhøj, Phys. Rev. A **36**, 3612 (1987).
[24] B. L. Schram, A. J. H. Boerboom, and J. Kistemaker, Physica (Amsterdam) **32**, 185 (1966).
[25] E. Krishnakumar and S. K. Srivastava, J. Phys. B **21**, 1055 (1988).
[26] H. Knudsen and J. F. Reading, Phys. Rep. **212**, 107 (1992).
[27] T. Kirchner, H. J. Lüdde, and R. M. Dreizler, Phys. Rev. A **61**, 012705 (1999).
[28] T. Kirchner, M. Horbatsch, and H. J. Lüdde, Phys. Rev. A **66**, 052719 (2002).
[29] T. Kirchner (private communication).
[30] E. C. Montenegro, W. E. Meyerhof, and J. H. McGuire, Adv. At., Mol., Opt. Phys. **34**, 249 (1994).
[31] J. H. McGuire, *Electron Correlation Dynamics in Atomic Collisions* (Cambridge University Press, Cambridge, England, 1997).
[32] E. C. Montenegro, A. C. F. Santos, W. S. Melo, M. M. Sant'Anna, and G. M. Sigaud, Phys. Rev. Lett. **88**, 013201 (2002).
[33] E. C. Montenegro and W. E. Meyerhof, Phys. Rev. A **43**, 2289 (1991).
[34] J. F. Babb and J. Shertzer, Chem. Phys. Lett. **189**, 287 (1992).
[35] B. Grémaud, D. Delande, and N. Billy, J. Phys. B **31**, 383 (1998).
[36] G. M. Sigaud and E. C. Montenegro, in *Photonic, Electronic and Atomic Collisions—XXII International Conference*, edited by J. Burgdörfer, J. S. Cohen, S. Datz, and C. Randy Vane (Rinton Press, Princeton, 2002), pp. 547–558.
[37] G. M. Sigaud and E. C. Montenegro, Braz. J. Phys. **33**, 382 (2003).
[38] N. V. de Castro Faria, I. Borges, L. F. S. Coelho, and G. Jalbert, Phys. Rev. A **51**, 3831 (1995).
[39] T. A. Carlson, W. E. Hunt, and M. O. Krause, Phys. Rev. **151**, 41 (1966).
[40] A. El-Shemi, Y. Lofty, and G. Zschornack, J. Phys. B **30**, 237 (1997).